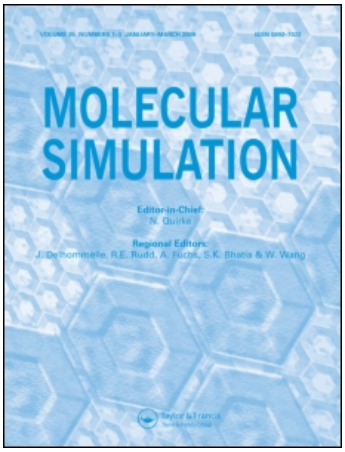

Molecular Simulation
Publication details, including instructions for authors and subscription information:
http://www.informaworld.com/smpp/title~content=t713644482

Atomistic Simulations of Rare Gas Transport through Breathable Single-wall Nanotubes with Constrictions and Knees

M. W. Roth[a]; J. Mesentseva[a]
[a] Department of Physics, University of Northern Iowa, Cedar Falls, IA, USA

To cite this Article Roth, M. W. and Mesentseva, J.(2004) 'Atomistic Simulations of Rare Gas Transport through Breathable Single-wall Nanotubes with Constrictions and Knees', Molecular Simulation, 30: 10, 661 — 667
To link to this Article: DOI: 10.1080/08927020410001722276
URL: http://dx.doi.org/10.1080/08927020410001722276

Molecular Simulation, Vol. 30 (10), 30 August 2004, pp. 661–667

Taylor & Francis
Taylor & Francis Group

Atomistic Simulations of Rare Gas Transport through Breathable Single-wall Nanotubes with Constrictions and Knees

M.W. ROTH* and J. MESENTSEVA

Department of Physics, University of Northern Iowa, Cedar Falls, IA 50614, USA

(Received July 2003; In final form April 2004)

We present the results of molecular dynamics (MD) computer simulations of rare gas diffusion through breathable nanotubes with pentagon–heptagon pair defects resulting in constrictions and knees. Diffusion involves interrupted high speed "choppy" motion with intermittent reversal in velocity direction. Single atoms exhibit a spiral-like path, in contrast to atoms traveling in groups. Considerable resistance to flow appears to reside in the upstream section of the nanotube where density gradients are small, prior to the constriction. Subsequently, considerable density gradients are present and speeds increase, becoming greatest at the tube exit. For the nanotubes examined, Kr and Xe diffusion was too hindered to provide reliable results. Diffusion of He through the nanotubes with knees occurs in a single-file fashion nearly along the center of the tube and the knee has no detectable effect on the diffusion kinetics. Transport diffusion coefficients are in the order of 10^{-4}–10^{-2} cm^2/s.

Keywords: Nanotube diffusion; Molecular dynamics; Rare gases; Permeation; Transport diffusivity

INTRODUCTION

Since their discovery in the early 1990s [1–3] nanotubes have been found to vary considerably in structure and dimension. As a result, arrays of carbon nanotubes present interesting and diverse environments in which to study equilibrium and non-equilibrium atomic and molecular processes. In particular, gradient-driven diffusion of various species through membranes is of considerable scientific and technological importance because of applications in gas separation and storage, in sorbent design and also in catalysis. There have been relatively few studies of atomic and molecular diffusion through various types of carbon nanotubes.

Tuzun and coworkers employ an MD technique to study the dynamics of He, Ar and C_{60} fluid flow through single wall nanotubes (SWNTs) [4,5]. They model flexible nanotubes with bond stretching and bending potentials, and all non-bonded interactions with Lennard–Jones (LJ) potentials. They find that incorporating the dynamic aspect of the nanotube is important because fluid–wall collisions slow the fluid down much more quickly in time than in a rigid tube. In addition, diffusing species with smaller mass flow more easily through the tubes. However, the fluid slowing depends on simulated time but not the length of the nanotube utilized. Overall, fluid flow through nanotubes is still poorly understood, and there is evidence that nanosystems could exhibit novel laminar/turbulent flow transitions with possible practical implications [6].

Not surprisingly, some of the first gas diffusion studies involve hydrocarbons. Düren and coworkers [7] use Dual Control Volume Grand Canonical Molecular Dynamics (DCV-GCMD) techniques [8] to calculate transport diffusion properties of CH_4/CF_4 mixtures in rigid nanotubes with three wall layers. Composition-dependent transport properties are calculated for driving pressure gradients four orders of magnitude larger than in corresponding real systems, but the calculated transport diffusivities are independent of the driving gradient. Mao and coworkers [9–11] model diffusion

*Corresponding author. Tel.: +1-319-273-7336. Fax: +1-319-273-7136. E-mail: rothm@uni.edu

ISSN 0892-7022 print/ISSN 1029-0435 online © 2004 Taylor & Francis Ltd
DOI: 10.1080/08927020410001722276

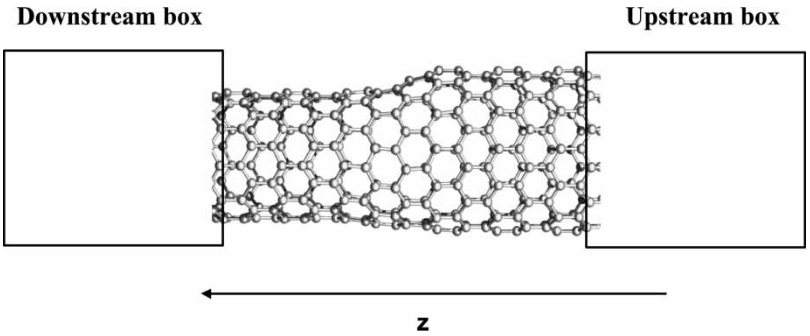

FIGURE 1 The computational cell utilized in this study, shown for the 120110 constricting nanotube. Note that the upstream and downstream boxes are placed slightly inside the tube in order to avoid leakage.

of various pure-component and mixed light alkane systems through breathable nanotubes and obtain reasonable diffusion coefficients. Skoulidas and coworkers conduct atomistically detailed MD simulations of H_2 and CH_4 [12] as well as Ar and Ne [13] through rigid SWNT arrays and find that transport diffusivities are orders of magnitude larger than those in silicalite with comparable pore size, possibly suggesting that SWNT arrays may represent a nearly ideal diffusion medium.

As computing facilities become increasingly robust, the application of new techniques even affording modeling methods other than direct numerical simulations are being developed [14]. In fact, the use of commercial MD codes and visualization software packages to model transport through nanotubes is commonplace in the molecular computing community [15]. Even so, the interesting few simulations of diffusion through nanotubes thus far involve straight and often rigid carbon structures. Therefore, much can be gained by embarking on a study of diffusion through breathable nanotubes which have defects resulting in constrictions and bends (knees). The purpose of the work at hand is to better understand the role that such topological entities have on the diffusion properties of rare gases through breathable nanotubes and to gain an idea of systematic changes in behavior vis-à-vis the dependence of various results on the type of diffusing species.

COMPUTATIONAL APPROACH

We employ an (N, V, T) MD method to simulate the transport of various gases through the nanotubes. Only single SWNTs are utilized because we desire to study the effects of elbows and constrictions, which could tend to blur in cases where a bundle of *breathable* tubes is used. Moreover, it seems unrealistic to expect experimental construction of a nanotube array with defects perfectly aligned. There are 100 rare gas atoms initially placed at random positions within an upstream, or high-pressure box such that they are no closer than 3 Å to one another. As a result of using only single tubes, efforts must be taken in order to increase atomic throughput so as to generate reliable results. In the interest of accelerating the simulations but yet capturing the diffusion dynamics within the tubes, we utilize very high pressures within the upstream box. Others have also used pressures orders of magnitude larger than encountered experimentally to increase flux for the diffusing species and hence achieve reliable statistics and calculation of diffusion coefficients in their simulations [7]. The box has perfectly reflecting walls with the exception of a circular hole which is coincident with the opening of the upstream end of the particular nanotube being studied. As the simulation proceeds, the rare gas diffuses through the nanotube along the z-direction and various quantities of interest are calculated. When a particular gas atom reaches the end of the tube it is placed randomly within the upstream box no closer than 3 Å to any other atom. Any center-of-mass motion of the nanotube is subtracted off as the simulation proceeds. Spurious rotational motion is also accounted for in a similar way, only using the nanotube's moment of inertia tensor and angular momentum. Temperature control is achieved by velocity rescaling for the rare gas and carbon atoms separately and a velocity Verlet algorithm with a time step $\Delta t = 0.0005$ ps is used to integrate the equations of motion. Runs are taken out to 10^5 time steps (50 ps). The computational cell is shown in Fig. 1.

Three types of nanotubes are used in our simulations. The (8,0)–(7,1) knee (8071) contains adjacent pentagon and heptagon defects which result in a bend of about 12°; the (9,0)–(5,5) knee (9055) is similar but has a 36° bend and the (11,0)–(12,0) (110120) hybrid has pentagon and heptagon edge-sharing defects that result in a constriction. Here the numbers within the parentheses are

nanotube chiral vectors. All the nanotubes used have interesting electronic properties and their structures were relaxed before their coordinates were obtained [16] and used in our MD program. Lambin *et al.* [16] and Ewals [17] provide further detailed information about them as well as other nanotubes with pentagon–heptagon pair defects. Representations of views of the various nanotubes used in this study are shown in Fig. 2.

There are several types of interaction potentials used in the simulations. The rare gas–rare gas potential as well as the rare gas–carbon potential are of a Lennard–Jones form,

$$u_{\mathrm{LJ}}(r_{ij}) = 4\varepsilon_{ij}\left[\left(\frac{\sigma_{ij}}{r_{ij}}\right)^{12} - \left(\frac{\sigma_{ij}}{r_{ij}}\right)^{6}\right], \tag{1}$$

where the potential parameters between various species are given in Table I; mixed interaction parameters are obtained with the use of Lorentz–Bertholot combining rules. In addition there is a non-bonded carbon–carbon interaction which is in a modified Lennard–Jones form whose parameters are also shown in Table I:

$$u_{\mathrm{LJ}}(r_{ij}) = \varepsilon_{\mathrm{CC}}\left[\left(\frac{\sigma_{\mathrm{CC}}}{r_{ij}}\right)^{12} - 2\left(\frac{\sigma_{\mathrm{CC}}}{r_{ij}}\right)^{6}\right]. \tag{2}$$

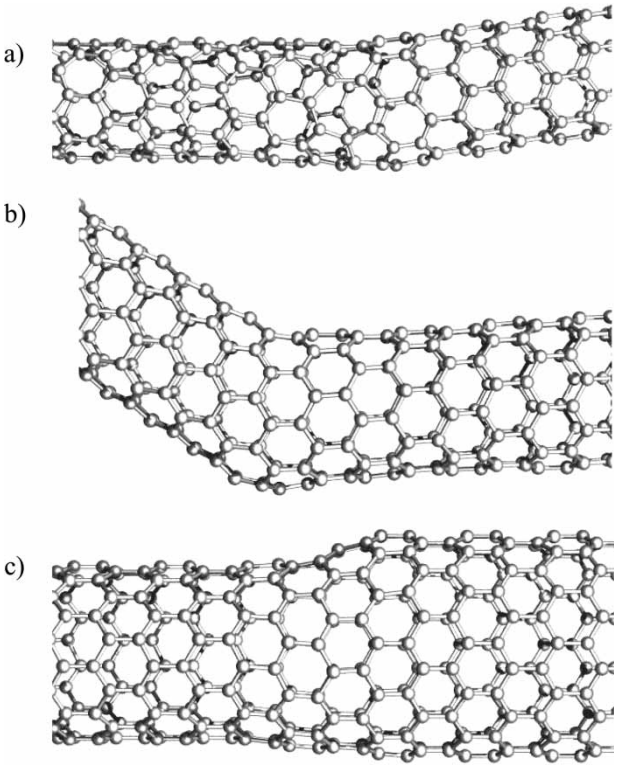

FIGURE 2 Representations of the (a) 8071, (b) 9055 and (c) 120110 nanotubes used in this study, to similar but not equal scales. Taken from Ref. [17].

TABLE I Parameters for the non-bonded Lennard–Jones interaction potentials

Species	ε_{ij} (K)	σ_{ij} (Å)
He—He	10.80	2.57
Ne—Ne	36.68	2.79
Ar—Ar	120.0	3.38
Kr—Kr	171.0	3.60
Xe—Xe	221.0	4.10
He—C	16.89	2.98
Ne—C	31.57	3.075
Ar—C	57.97	3.19
Kr—C	69.19	3.5
Xe—C	78.66	3.75
C—C	34.839	3.805

The carbon–carbon bonded interactions are modeled by Brenner's empirical extended bond-order potential [18]

$$\begin{aligned} V_{\mathrm{R}}(r_{ij}) &= f(r_{ij})\frac{D_e}{S-1}\exp\left[-\beta\sqrt{2S}(r-R_e)\right] \\ V_{\mathrm{A}}(r_{ij}) &= f(r_{ij})\frac{D_e S}{S-1}\exp\left[-\beta\sqrt{\frac{2}{S}}(r-R_e)\right] \\ f(r_{ij}) &= \begin{cases} 1, & r \le R_1 \\ \frac{1}{2}\left[1+\cos\left(\frac{(r_{ij}-R_1)\pi}{(R_2-R_1)}\right)\right], & R_1 < r_{ij} < R_2 \\ 0, & r_{ij} \ge R_2 \end{cases} \end{aligned} \tag{3a}$$

which has parameters that are fit to various energetics of hydrocarbons, diamond and graphite. In Eq. (3a), V_{R} and V_{A} are the repulsive and attractive terms, respectively, which are essentially modified Morse potentials. The screening function $f(r_{ij})$ restricts the interaction to the nearest neighbors as defined by the values for R_1 and R_2. In addition, the Brenner potential takes bonding topology into account with the empirical bond order function $\bar{B}_{ij}$ given by the relationships

$$\begin{aligned} B_{ij} &= 1 + \left[\sum_{k\neq i,j}^{N} G_{\mathrm{C}}(\theta_{ijk}) f(r_{ik})\right]^{-\delta} \\ G_{\mathrm{C}}(\theta) &= a_0\left[1 + \frac{c_0^2}{d_0^2} - \frac{c_0^2}{d_0^2 + (1+\cos\theta)^2}\right] \\ \bar{B}_{ij} &= \frac{B_{ij} + B_{ji}}{2}. \end{aligned} \tag{3b}$$

Variations of the Brenner potential have been used for many different types of carbon allotrope simulations, as the empirical bond order function controls clustering to some extent. The entire

TABLE II Parameters for the bonded carbon–carbon Brenner interaction potential

Parameter	*Value*
D_e	73333.33 K
β	1.5/Å
S	1.29
R_e	1.315 Å
R_1	1.750 Å
R_2	2.000 Å
δ	0.80469
a_0	0.011304
c_0	19
d_0	2.5

carbon–carbon interaction is a sum over all bonded and non-bonded interactions:

$$u_{CC} = \sum_{i=1}^{N} \sum_{j>i}^{N} \left\{ [V_R(r_{ij}) - \bar{B}_{ij} V_A(r_{ij})] + P_{ij} u_{LJ}(r_{ij}) \right\}. \quad (4)$$

Here P_{ij} is a screening function [19] which we implement by creating bonded and non-bonded neighbor lists. All carbon–carbon bonded potential parameters are given in Table II.

RESULTS AND DISCUSSION

Most of the calculations are done for the 110120 junction which has a constriction, as shown in Fig. 2. Unless otherwise noted, the following discussion refers to simulations at $T = 1500$ K which exhibit behavior typical of the system at other temperatures. Figure 3 shows the number of atoms N_t which reach the end of the nanotube plotted against simulation time (throughput) and Fig. 4 shows the loading, or number of atoms residing within the tube also as a function of simulation time for He, Ne and Ar. The throughput of Xe and Kr are so small as to yield statistically unreliable results—typically 1 and 0 atoms in 50 ps, respectively. As desired, the system reaches equilibrium loading relatively early. Even as loading is taking place, atoms begin to exit the tube and, remarkably, the rate of atomic throughput (the slope of the lines in Fig. 3) is established very early in the simulations, allowing reliable calculation of transport diffusion coefficients.

In the previous work on gradient-driven diffusion of hydrocarbons through zeolites [20], we used GCMC to fix the chemical potential in the upstream and downstream cells. On the low-pressure side, the molecules were instantly destroyed after they exited the zeolite, and were created in the high-pressure box when they entered the zeolite. In steady state, the number of diffusing particles was constant in both the high-pressure cell and the zeolite channels and there were none on the low-pressure side. Moreover, there were no control volumes either inside the zeolite or in contact with the zeolite surface. Therefore, in steady state such GCMC simulations and our present nanotube simulations act in an identical fashion. Our simulations may be viewed very crudely as GCMC simulations where an initially unknown chemical potential in the upstream box is arrived at in a self-consistent manner.

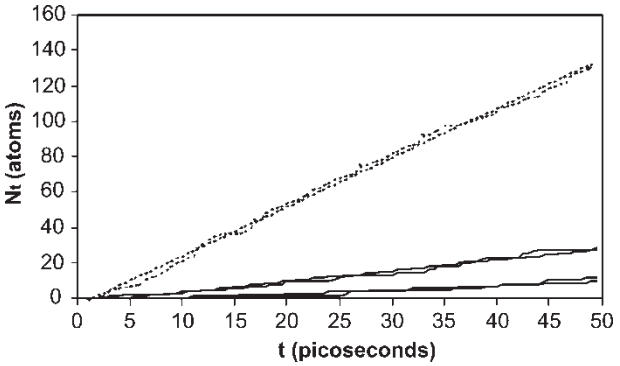

FIGURE 3 Atomic throughput N_t vs. simulated time at $T = 1500$ K for He (dashed), Ne (regular black) and krypton (bold). The best linear fits are also shown, the slopes m_t of which are listed in Table III.

During equilibration there is also a transient time for the nanotubes to adjust which is considerably shorter than the diffusion equilibration time described above. Simulations which are 10^6 time steps (500 ps) in length have been run to check the stability of the atomic throughput rate and the results of such simulations show no significant differences from the ones being discussed here. It is interesting to note that the throughput rates depend strongly on the type of diffusing species, but the equilibrium loading changes very little from one species to another. Table III shows equilibrium loadings and throughput rates for various species and temperatures. The temperature dependence of throughput rate for a given species is not surprising. Examination of equilibrium loadings in Table III, density

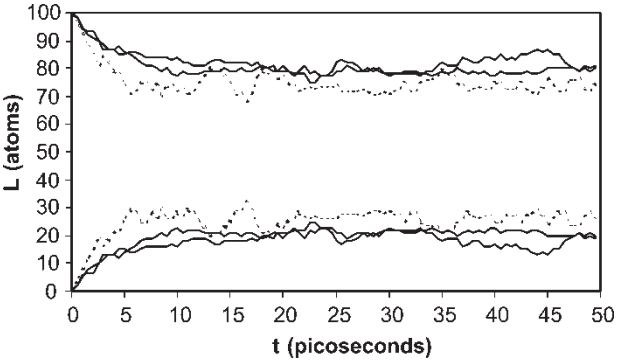

FIGURE 4 Number of atoms in the high pressure box (upper curves) and nanotube atomic loading L (lower curves) vs. simulation time at $T = 1500$ K for He, Ne and Ar in the same format as that for Fig. 3. Note that, since L is assigned a symbol, it is the only variable appearing on the y-axis title.

TABLE III Calculated throughput rate, loading, estimates of the upstream box pressure as calculated with the ideal gas law, flux, average density gradient within the nanotube and diffusion coefficients for various species diffusing through 120110 nanotube at different temperatures

Species/temperature (K)	m_t *(atom/ps)*	*L (atom)*	*P (atom)*	J_x *(cm²/s)*	$\Delta\rho$ *(× 10⁴ mol/m³)*	D_t *(cm²/s)*
He/300	1.76	20.87	789	413.40	1.65	7.53×10^{-3}
He/500	1.98	20.64	1320	465.08	1.82	7.69×10^{-3}
He/700	2.20	20.6	1850	516.76	1.95	7.96×10^{-3}
He/900	2.40	21.73	2340	563.73	1.85	9.18×10^{-3}
He/1500	2.80	26.22	3680	657.69	1.92	1.03×10^{-2}
He/2000	2.20	28.04	4790	516.76	1.82	8.55×10^{-3}
Ne/300	0.2	21.35	785	46.98	1.89	7.46×10^{-4}
Ne/500	0.2	22.29	1290	46.98	1.87	7.56×10^{-4}
Ne/1500	0.6	18.44	4070	140.93	2.09	2.02×10^{-3}
Ne/2000	0.42	25.5	4950	98.65	2.58	1.15×10^{-3}
Ar/300	0.052	19.27	805	12.214	2.16	1.70×10^{-4}
Ar/500	0.122	20.87	1320	28.66	2.04	4.23×10^{-4}
Ar/1500	0.22	21.24	3930	51.68	2.02	7.72×10^{-4}
Ar/2000	0.4	21.31	5230	93.96	2.65	1.07×10^{-3}

profiles and velocity profiles within the tube (not shown here but to be defined later) reveal that the decrease in throughput for He and Ne is a result of resistance to flow through considerably high loading in the tube resulting in congestion at the constriction.

Figure 5 shows velocity profiles at 1500 K for He, Ne and Ar. The velocity profile is calculated by averaging the velocity that all atoms in each length interval of 0.3 Å have. The velocity profiles reveal that attraction toward the tube opening begins well into the upstream box. Prior to entering the tube, there is a slight jump in atomic speed followed by a slight decrease, signaling increased attraction toward the upstream opening followed by slight resistance. Such effects are more prominent for lower mass species despite weaker interaction with the nanotube. Upon entering the tube there is a dramatic increase in average speed compared to that in the high-pressure box, as well as in fluctuations in the profile, indicating rapid, choppy diffusive motion. Inspection of animation sequences confirm such interrupted diffusive motion, and in fact shows that there are instances when atoms reverse for some small time before proceeding downstream.

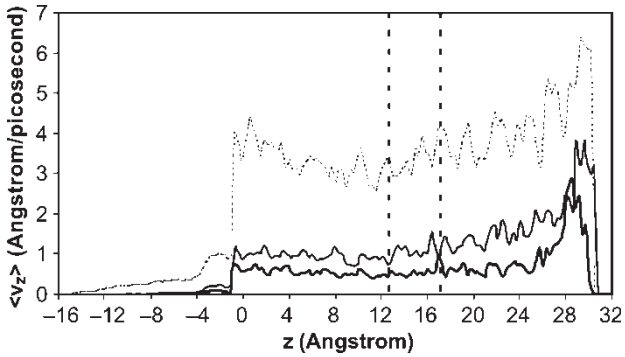

FIGURE 5 Velocity profiles at $T = 1500$ K along the diffusion direction for He, Ne and Ar with the same legend as in Fig. 3. Dotted lines indicate the region over which the tube constricts.

The average velocity decreases somewhat until the constriction is reached, due to collisions (scattering) with the nanotube walls. The decrease is more prominent for helium, indicating that the diffusate–carbon interactions are very influential on the system. In other words, even though helium has the weakest interaction with the tube walls, its low mass results in a large effect on the diffusing motion. Examination of the velocity profiles for gases with higher masses serves as a confirmation of such an idea. After encountering the constriction, average velocity tends to become larger, with an abrupt increase at the tube's end, indicating that the atoms exit the tube very rapidly. Simulated motion pictures of the simulations reveal that, at the end of the tube, the atoms are kicked out by other atoms right behind. At lower temperatures the change in velocity at exit is more abrupt, as it also is for Xe, suggesting that, in the latter case, tube deformation may be playing some role for larger species when they are knocked out. We examined distributions for all components of the velocity and did not find evidence for a spiral-like diffusion path. However, the diffusion path of single atoms through the tube are spiral-like, as evidenced by the plot of v_y vs. v_x in Fig. 6. The curves whose points are farther out from the center (indicating larger speeds) correspond to motion in the larger part of the tube (prior to the constriction) and the curves closer to the origin correspond to motion after the atom has encountered the constriction. Although not perfectly circular, the curves suggest that diffusive motion takes place along a path very similar to a spiral. Examination of animations of the simulation confirms such a notion. Mao *et al.* [19] predict a spiral diffusion path for non-spherical organic molecules in certain nanotubes, and also find that as loading increases the spiral nature of the path becomes less prominent due to interactions between the diffusing atoms.

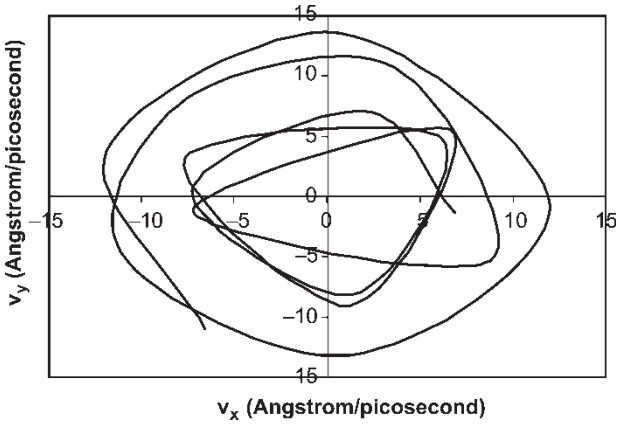

FIGURE 6 Velocity profile in the plane perpendicular to the direction of diffusion for a single atom of helium at $T = 300\,\mathrm{K}$.

Figure 7(a) shows the density profiles at 1500 K for He, Ne and Ar with different vertical axes in order to emphasize features of the profile within the tube itself. The density profile is calculated as the average number of atoms within the same length intervals that the velocity profile is partitioned on. The choice of diffusing species has little effect on the density profile, as confirmed by the equilibrium loading data in Table III. There are small peaks in the density on the upstream side, consistent with the notion of slight resistance to entry there. Inside the tube there is level density up until the constriction, after which a density gradient is established up until the downstream end of the tube. Such a picture is consistent with the notion that most of the resistance to flow is encountered on the upstream side of the constriction, and that the constriction is responsible for blocking the flow somewhat, even on an atomic level. Such a picture is also consistent with the diffusivities for Ne being less at $T = 2000\,\mathrm{K}$ than at $T = 1500\,\mathrm{K}$, and for He being less at $T = 2000\,\mathrm{K}$ than even at $T = 900\,\mathrm{K}$ because the constriction augments the sensitivity of diffusion to increased loading. The snapshot of diffusion through the 120110 tube in Fig. 8 reveals that there is diffusate congestion due to the constriction.

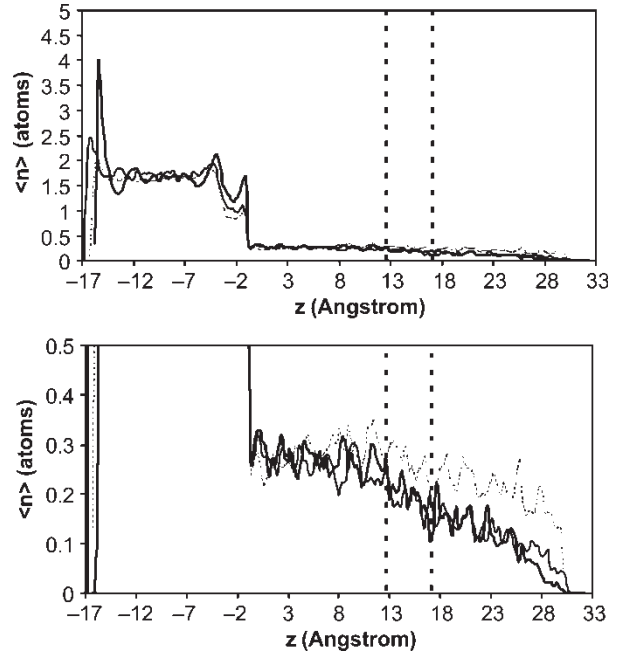

FIGURE 7 Density profiles at $T = 1500\,\mathrm{K}$ along the diffusion direction for He, Ne and Ar in the same format as that for Fig. 5, but with (top) full vertical scale and (bottom) reduced vertical scale to facilitate illustration of certain features of the profiles within the tubes.

Simulations were also conducted with 8071 and 9055 nanotubes with knees, as shown in Fig. 8. We find that diffusion for even Helium occurs in an interrupted, choppy single file manner in the 8071 tube. In the slightly larger 9055 hybrid, there is some congestion at the elbow but the situation is nearly the same for both tubes—as long as diffusion takes place in single file the bend does not affect diffusion kinetics. We suspect that the knees for larger tubes could serve as shape/size selectors, and that they could have a profound effect on diffusion kinetics, especially for high loadings.

The transport diffusivity, D_t, is defined as

$$\vec{J} = -D_\mathrm{t}\vec{\nabla}c, \tag{5}$$

where $\vec{J}$ is the flux and c is the concentration of diffusing species. Since we encounter diffusion in mainly one direction the flux J_x is defined here to be the slope m_t of the throughput line divided by the average cross-sectional area of the nanotube: $J_x = (m_t/A)$. For diffusion in one dimension, then, D_t is given by

$$D_\mathrm{t} = \frac{J_x}{\left(\frac{\Delta\rho}{\Delta x}\right)_{nanotube}}. \tag{6}$$

Here the quantity in the denominator is taken to be the average slope of the density profile within the nanotube. Values for throughput rates m_t as calculated from the slopes of throughput curves, fluxes J_x, upstream densities and diffusion coefficients for various species diffusing through the 110120 nanotube with a constriction are shown in Table III. For the simulations involving nanotubes with knees, the single file diffusion resulted in a sufficiently low throughput that the diffusion coefficients are felt to be unreliable. We suspect that, for larger tubes with knees, congestion will play a much more significant role, and especially at higher loadings. Our diffusion coefficients for the 110120 fit in reasonably with those calculated for other systems diffusing in various straight nanotubes: they are comparable to those calculated by Düren *et al.* for CH_4/CF_4 [7], larger than for methane/ethylene by Mao [21] and smaller than those calculated for rare gases by Ackerman, who to

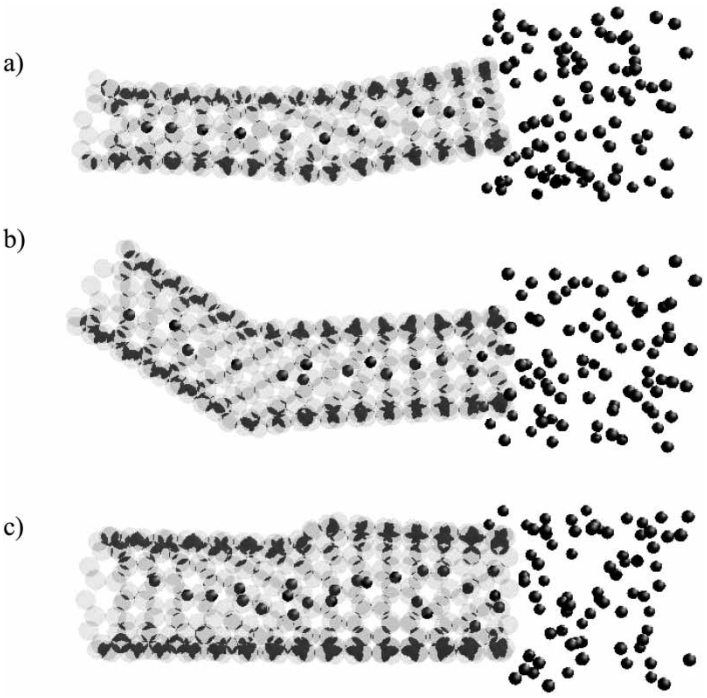

FIGURE 8 Snapshots of diffusion through (a) 8071, (b) 9055 and (c) 120110 nanotubes.

the best of our knowledge use static nanotubes [13] which may elevate diffusion coefficients due to the importance of diffusate–tube interactions [4,5].

Acknowledgements

The first author gratefully acknowledges illuminating discussions with J. Che. Both authors are grateful to the University of Northern Iowa for support of this work through a summer 2002 undergraduate research fellowship.

References

[1] Iijima, S. (1991) "Helical microtubules of graphitic carbon", *Nature* **354**, 56.
[2] Iijima, S. and Ichihashi, T. (1993) "Single-shell carbon nanotubes of 1-nm diameter", *Nature* **363**, 603.
[3] Bethune, D.S., Kaing, C.H., de Vries, M.S., Gorman, G., Savoy, R., Vazquez, J. and Beyers, R. (1993) "Cobalt-catalyzed growth of carbon nanotubes with single-atomic-layer walls", *Nature* **363**, 605.
[4] Tuzun, R.E., Noid, D.W. and Sumpter, B.G. (1996) "Dynamics of fluid flow inside carbon nanotubes", *Nanotechnology* **7**, 241.
[5] Tuzun, R.E., Noid, D.W. and Sumpter, B.G. (1997) "Dynamics of He/C_{60} flow inside carbon nanotubes", *Nanotechnology* **8**, 112.
[6] Tuzun, R.F., Newman, D.E., Noid, D.W. and Sumpter, B.G. "Atomistic fluid flow transitions inside carbon nanotubes", *Fifth Foresight Conference on Molecular Nanotechnology.*
[7] Düren, T., Kiel, F.J. and Seaton, N.A. (2002) "Composition dependent transport diffusion coefficients of CH_4/CF_4 mixtures in carbon nanotubes by non-equilibrium molecular dynamics simulations", *Chem. Eng. Sci.* **57**, 1343.
[8] Heffelfinger, G.S. and van Swol, F. (1994) "Diffusion in Lennard–Jones fluids using dual control volume grand canonical molecular dynamics simulation (DCV-GCMD)", *J. Chem. Phys.* **100**(10), 7548.
[9] Mao, Z., Garg, A. and Sinnott, S.B. (1999) "Molecular dynamics simulations of the filling and decorating of carbon nanotubules", *Nanotechnology* **10**, 273.
[10] Mao, Z. and Sinnott, S.B. (2000) "A computational study of molecular diffusion and dynamic flow through carbon nanotubes", *J. Phys. Chem. B* **104**, 4618.
[11] Mao, Z. and Sinnott, S.B. (2001) "Separation of organic molecular mixtures in carbon nanotubes and bundles: molecular dynamics simulations", *J. Phys. Chem. B* **105**, 6916.
[12] Skoulidas, A.I., Ackerman, D.M., Johnson, J.K. and Scholl, D.S. (2002) "Rapid transport of gases in carbon nanotubes", *Phys. Rev. Lett.* **89**, 185901.
[13] Ackerman, D.M., Skoulidas, A.I., Sholl, D.S. and Johnson, K.J. (2003) "Diffusivities of Ar and Ne in carbon nanotubes", *Mol. Simulation* **29**, 684.
[14] Lam, R., Vlachos, D.G. and Katsoulakis, M.A. (2002) "Homogenization of mesoscopic theories: effective properties of membranes", *AIChE J.* **48**(5), 1083.
[15] Cohen, J., Zhu, F. and Tajkhorshid, E. (2003) "Simulation of water permeation through nanotubes", web tutorial, http://www.ks.uiuc.edu/Training/SumSchool03/Tutorials/nanotubes.
[16] Lambin, P.h. and Meunier, V. (2002) "Connecting carbon nanotubes with pentagon–heptagon pair defects", electronic structure archive, http://www.fundp.ac.be/(phlambin/Nanotube/knee.html, Nanotechnology White Paper Library, NanoBusiness Alliance, Inc.
[17] Ewals, C. (2003) "Joining nanotubes with pentagons and heptagons", http://www.hpc.susx.ac.uk/(ewels/img/science/kinked/, ray-traced image gallery.
[18] Brenner, D.W. (1990) "Empirical potential for hydrocarbons for use in simulating the chemical vapor deposition of diamond films", *Phys. Rev. B* **42**(15), 9458.
[19] Che, J., Çagin, T. and Goddard, W.A. (1999) "Studies of fullerenes and carbon nanotubes by an extended bond order potential", *Nanotechnology* **10**, 263.
[20] Chandross, M., Webb, E.B., Grest, G.S., Martin, M.G., Thompson, A.P. and Roth, M.W. (2001) "Dynamics and exchange at gas–zeolite interfaces I: pure component butane and isobutane", *J. Phys. Chem. B* **105**(24), 5700–5712.
[21] Mao, Z. and Sinnott, S.B. (2002) "Prediction of a spiral diffusion path for nonspherical organic molecules in carbon nanotubes", *Phys. Rev. Lett.* **89**(27), 278301.